Acta Cryst. (1979). A35, 201–213

X-ray Interferometry with Divergent Polychromatic Beams

BY E. V. SHULAKOV AND V. V. ARISTOV

Solid State Physics Institute, Academy of Sciences of the USSR, Moscow District, Chernogolovka 142432, *USSR*

(*Received* 24 *June* 1977; *accepted* 8 *August* 1978)

Abstract

The theory of a strongly absorbing Laue interferometer for an arbitrary composition of the X-radiation has been developed on the basis of the Takagi equations. The coherent properties of interfering beams of polychromatic radiation are discussed. Formulas have been derived showing the dependence on the moiré pattern and the contrast of interference fringes of the type of deviation of the interferometer geometry from the perfectly aligned case. The results of an experiment for obtaining the moiré pattern of a symmetric Laue case (LLL) interferometer with *Bremsstrahlung* radiation are presented.

Analysis of the X-ray interferometer operation is usually carried out on the assumption that the radiation incident on a crystal is monochromatic (Pinsker, 1974). It is known from optical interferometry that interference fringes may be observed not only with monochromatic but also with white light (Born & Wolf, 1964). Such an interference pattern appears, for instance, in the Jamin interferometer, which resembles X-ray interferometers. It is also expected that interference with X-ray 'white' radiation may be observed by X-ray interferometers. The consideration of such a problem seems to be interesting from the viewpoint of diffraction theory and also for a possible extension of the region of X-ray interferometer application.

The present work analyses the conditions for the existence of interference with polychromatic radiation. The moiré patterns produced by a focused interferometer are shown to be similar to those observed using monochromatic radiation. The effect of defocusing on the visibility of the polychromatic interference fringes is considered. An experiment is described which is carried out with a symmetric Laue-case interferometer (LLL interferometer, Bonse & Hart, 1965); the results confirm the possibility of obtaining a diffraction moiré pattern with polychromatic radiation.

1. Diffraction of polychromatic radiation by the LLL interferometer

When considering the diffraction of polychromatic radiation by an interferometer we use the method proposed by Aristov, Shmytko & Shulakov (1977*a*) for analysing the contrast of a perfect-crystal topographical image. The essence of this method is that the radiation of a polychromatic point source expands into spherical monochromatic waves, the intensities of each of these waves being calculated at all points of the film after their diffraction by the crystal. The total intensity is obtained by integrating over the range of wavelengths which contribute to the image at the given point.

Fig. 1 is a diagram of the diffraction of a divergent polychromatic beam by the LLL interferometer. The

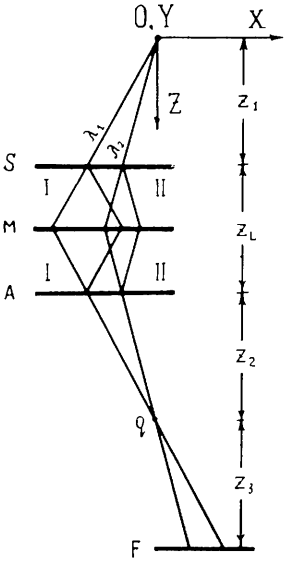

Fig. 1. The diffraction of a divergent polychromatic beam by the LLL interferometer. *O* is the point source of radiation; *S*, *M*, *A* are wafers of the interferometer; I and II denote the first and second paths of the interfering waves; *XYZ* is the orthogonal coordinate system in use, with origin at the point *O*; **OX** is parallel to the normal to reflecting planes; **OZ** is normal to the surface of the interferometer wafers; *q* is the focusing point of the beams with different wavelengths; *F* is the photographic film; z_1 is the distance from the radiation source to the interferometer; z_L is the interferometer size; z_2 is the distance from the interferometer to the focusing point q ($z_2 = z_1$); z_3 is the distance from the focusing point to the film ($-z_2 \leq z_3 < \infty$); at $z_3 > 0$ the image on the film is inverted.

0567-7394/79/010201-13$01.00

conditions for Bragg diffraction are satisfied for each wavelength for a very narrow range of $\Delta\theta_o$ angles (for a thick, strongly absorbing crystal $\Delta\theta_o \lesssim 10^{-5}$ rad), and we may thus consider each point $\mathbf{r}_{S1}(x_{S1},y_{S1},z_{S1})$ of the entrance surface of the first interferometer wafer to correspond to a certain wavelength determined from the condition:

$$\tan\theta = -x_{S1}\cos\psi/z_1, \tag{1}$$

where θ is the Bragg angle, and ψ is the angle between the diffraction plane and the plane $y = 0$.*

As a result of diffraction by all the interferometer wafers, each of the monochromatic components of the wavefield extends in the manner shown in Fig. 2, and the wavefield at the exit interferometer surface corresponding to the wavefield at the point $\mathbf{r}_{S1}$ has the same wavelength but has a noticeable intensity over a region of width of the order of $2T\tan\varepsilon_m/\cos\psi$, where $T = t_S + t_M + t_A$ is the total thickness of the interferometer slabs, and $2\varepsilon_m$ is the angular width of the monochromatic wavefield in the crystal with thickness $T/\cos\psi$ (for the 220 reflection of Si at $\lambda \simeq 1{\cdot}54$ Å, $T = 1{\cdot}5$ mm, $\cos\psi \simeq 1$ $T\tan\varepsilon_m$ is about 200 μm).†

* Usually, the size of the irradiated area of an interferometer is much less than the distance z_1. In this case $\cos\psi \simeq 1$ and the wavelength of the diffracted rays varies in the **OX** direction only (for the equation of the curves for λ = constant see, for instance, Aristov & Shulakov, 1975).

† Here and below for quantitative estimates we use the interferometer parameters and geometry of the experiment by Bonse & Hart (1965): the 220 reflection of Si, Cu $K\alpha$ radiation ($\lambda = 1{\cdot}54$ Å), $T = 1{\cdot}5$ mm, $\cos\psi \simeq 1$, $z_1 \simeq -z_3 \simeq 500$ mm.

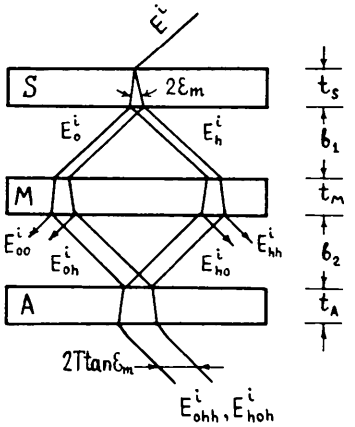

Fig. 2. Scheme of the monochromatic spherical-wave diffraction by the LLL interferometer. t_S, t_M and t_A are the thicknesses of the S, M and A wafers ($t_S + t_M + t_A = T$); b_1 and b_2 are the widths of air gaps between the wafers of the interferometer; $2\varepsilon_m$ is the angular width of the Borrmann triangle in an absorbing crystal; indices o and h at amplitudes E^i denote the beams propagating in the directions of the reciprocal-lattice points o and h after diffraction by S, M and A wafers.

Let us choose a narrow wavelength range $d\lambda$ such that the variation of the diffraction angle $d\theta$ with a change in the wavelength should be much less than the angular width of reflection $\Delta\theta_o$ for a monochromatic wave:

$$d\theta = (d\lambda/\lambda)\tan\theta \ll \Delta\theta_o. \tag{2}$$

The fulfilment of this condition permits one to assume the field inside the range $d\lambda$ to be monochromatic, and to calculate the linear density of intensity $di_h(\lambda,\mathbf{r}_{A2})$ in this wavelength range at the point $\mathbf{r}_{A2}(x_{A2},y_{A2},z_{A2})$ of the exit surface of the interferometer wafer A ($z_{A2} = z_1 + z_L$):*

$$di_h(\lambda,\mathbf{r}_{A2}) = (c/8\pi)\sigma(\lambda)|E_h^{\mathrm{I}}(\lambda,\mathbf{r}_{A2}) + E_h^{\mathrm{II}}(\lambda,\mathbf{r}_{A2})|^2 d\lambda. \tag{3}$$

Here $\sigma(\lambda)$ is the spectral density of radiation, c is the velocity of light, E_h^{I} and E_h^{II} are the amplitudes of monochromatic waves travelling by paths I and II and propagating in the direction of the reciprocal-lattice point h.

Let us determine the intensity distribution $dI_h(\lambda,\mathbf{r}_F)$ for the range $d\lambda$ at the point $\mathbf{r}_F(x_F,y_F,z_F)$ on the film located at a distance $z_2 + z_3$ from the interferometer ($z_F = z_1 + z_L + z_2 + z_3$). The structure of a diffraction image varies slowly in the diffraction plane with distance $z_2 + z_3$ increasing owing to a negligible angular divergence of the diffracted rays $\Delta\theta_o$. This variation in the image structure may be neglected until $(z_2 + z_3) \ll 2T\tan\varepsilon_m/\Delta\theta_o\cos\psi \simeq 40$ m and it may be considered that the wavefield at each point $\mathbf{r}_{A2}$ corresponds to that at the point $\mathbf{r}_F$ which lies at the intersection of the ray, traced from the point $\mathbf{r}_{A2}$ parallel to the wavevector of the diffracted beam $E_h^{\mathrm{I(II)}}$, and the film plane. Because of the parallel transfer of the wavefield in the diffraction plane from the interferometer exit surface to the film, the intensity distribution $dI_h(\lambda,\mathbf{r}_F)$ is a replica of the intensity distribution $di_h(\lambda,\mathbf{r}_{A2})$ in this diffraction plane, with the coordinates of the points $\mathbf{r}_f$ and $\mathbf{r}_{A2}$ related to the experimental geometry by the conditions:

$$x_F = x_{A2} + (z_2 + z_3)\tan\theta/\cos\psi,$$
$$y_F = m_y y_{A2}. \tag{4}$$

Here $m_y = z_F/z_{A2}$ is the image magnification factor in the **OY** direction. Because of divergence of the diffracted waves in the **OY** direction the intensity on the film is m_y times less than that on the exit surface of the A wafer; therefore,

$$dI_h(\lambda,\mathbf{r}_F) = m_y^{-1}\, di_h(\lambda,\mathbf{r}_{A2}). \tag{5}$$

* The dependence of the spectral density of the intensity on the wavelength at the point $\mathbf{r}_{A2}$ is shown in equation (A.16). Intensity $di_h(\lambda,\mathbf{r}_{A2})$ is obtained by multiplication of the right-hand side of equation (A.16) by $d\lambda$.

For polychromatic beam diffraction by an interferometer, the wavefield intensities with different λ are superimposed at each point $\mathbf{r}_F$ of a film. The range of wavelengths contributing to the total intensity at the observation point is determined by the width of the monochromatic beams ($2T\tan\varepsilon_m/\cos\psi$), the interferometer defocusing ($\Delta b = b_2 - b_1$) (usually, $|\Delta b| \lesssim$ 10–20 μm), and the experimental geometry. It may be considered that only those rays are incident upon the point $\mathbf{r}_F$ for which the following condition is fulfilled (Aristov *et al.*, 1977*a*):

$$\tan\theta = (x_F - x_q)\cos\psi/z_3. \qquad (6)$$

Here $x_q - \Delta b\tan\theta/\cos\psi$ and $x_q + \Delta b\tan\theta/\cos\psi$ are zero at the centres of the monochromatic beams E_h^{I} and E_h^{II}, and the variable x_q changes within the ranges $|x_q\cos\psi - \Delta b\tan\theta| \lesssim T\tan\varepsilon_m$ and $|x_q\cos\psi + \Delta b\tan\theta| \lesssim T\tan\varepsilon_m$ respectively. In terms of x_q, the x coordinates of $\mathbf{r}_F$ and $\mathbf{r}_{A2}$ are related by the condition: $x_F = -m_x x_{A2} + (1 + m_x)x_q$, where $m_x = z_3/z_2$ is the image magnification factor in the **OX** direction. From equation (6) it also follows that the beams $E_h^{\mathrm{I}}(\lambda,\mathbf{r}_F)$ and $E_h^{\mathrm{II}}(\lambda,\mathbf{r}_F)$ of all wavelengths focus at $z_3 = 0$ in the range $|x_F| \lesssim (T\tan\varepsilon_m + |\Delta b|\tan\theta)/\cos\psi \simeq$ 200–220 μm.

Let us determine the intensity distribution $I_h(\mathbf{r}_F)$, having integrated expression (5) over all wavelengths. On integrating it is convenient to substitute variable λ by x_q, using the relation (6) and the Bragg equation $2d_h\sin\theta = \lambda$:

$$x_q = x_F - \lambda z_3/2d_h\cos\theta\cos\psi,$$
$$\mathrm{d}x_q = -(z_3/2d_h\cos^3\theta\cos\psi)\mathrm{d}\lambda. \qquad (7)$$

Changing the variables and integrating, we get:

$$I_h(\mathbf{r}_F) = \frac{c}{8\pi m_x m_y}\int_{-\infty}^{\infty}\sigma(x_q,\mathbf{r}_F)|E_h^{\mathrm{I}}(x_q,\mathbf{r}_F) + E_h^{\mathrm{II}}(x_q,\mathbf{r}_F)|^2\mathrm{d}x_q, \qquad (8)$$

where $\sigma(x_q,\mathbf{r}_F) = \sigma(\mathbf{r}_{S1}) = (2d_h\cos^3\theta\cos\psi/z_1)\sigma(\lambda)$ is the linear density of radiation diffracted at the point $\mathbf{r}_{S1}$ of the entrance surface of the S wafer and incident upon the point of observation $\mathbf{r}_F$ [points $\mathbf{r}_{S1}$ and $\mathbf{r}_F$ are connected by equations (1) and (6) and $y_{S1} = y_F z_1/z_3$; $\tan\psi = y_F/z_F$].

Thus, intensity $I_h(\mathbf{r}_F)$ in the case of polychromatic radiation can be found by determining the distribution of fields $E_h^{\mathrm{I(II)}}(x_q,\mathbf{r}_F)$ for the monochromatic wave. The formation of an X-ray moiré pattern by monochromatic radiation has been investigated by many authors. It is known that the contrast of the interference pattern depends on the character of the interferometer deflection from the ideal one, on the total absorption value, and so on. Below, we shall assume the interferometer to be strongly absorbing. Such an assumption is usually well justified in experiment; for instance, Pinsker (1974) considers a silicon interferometer with $\mu T = 22$ (μ is the linear coefficient of the X-ray photoelectric absorption) as a typical example.* A calculation of fields $E_h^{\mathrm{I(II)}}(x_q,\mathbf{r}_F)$ in the strong-absorption approximation is presented in Appendix *A*. It is carried out on the basis of a generalized dynamic theory (Takagi, 1962; Indenbom & Chukhovsky, 1972).

As follows from equation (*A*.17), in this approximation we obtain:

$$|E_h^{\mathrm{I(II)}}(x_q,\mathbf{r}_F)|^2 = |\chi_h|^2|P_1(x_q,\mathbf{r}_F)|^2|P_2(x_q,\mathbf{r}_F)|^2 \times \exp[-(x_q \mp \Delta b\tan\theta/\cos\psi)^2/\Delta_o^2]. \qquad (9)$$

Here $P_1(x_q,\mathbf{r}_F) = P_1(\lambda,T/\cos\psi)$ and $P_2(x_q,\mathbf{r}_F) = P_2(\lambda,z_1/\cos\psi)$ [see equations (*A*.5*b*) and (*A*.7); values θ and λ in $P_1(\lambda,T/\cos\psi)$ and $P_2(\lambda,z_1/\cos\psi)$ are determined by the coordinates of the observation point $\mathbf{r}_F$ and the variable x_q]; Δ_o is determined by equations (*A*.12) and (*A*.5) and equals $(\lambda T\sin^2\theta/\pi|\chi''|\cos\theta\cos\psi)^{1/2}$ [χ'' is the imaginary part of $\chi = (\chi_h\chi_{\bar{h}})^{1/2}$, where χ_h and $\chi_{\bar{h}}$ are the h and $\bar{h}$ Fourier expansion coefficients of the crystal polarizability].

It can be seen from equation (9) that the intensities of wavefields E_h^{I} and E_h^{II} have significant values in the region $|x_q \mp \Delta b\tan\theta/\cos\psi| \lesssim \Delta_o$ only. It follows, therefore, that the range of wavelengths $\Delta\lambda$, whose intensities are summed at each point $\mathbf{r}_F$, is limited:

$$\Delta\lambda/\bar{\lambda} \simeq 2(\Delta_o\cos\psi + |\Delta b|\tan\theta)\cos^2\theta/|z_3|\tan\theta, \qquad (10)$$

where $\bar{\lambda}$ is the mean value of λ for this range; $\bar{\lambda}$ is determined by equation (6) at $x_q = 0$. When $|z_3| \lesssim \Delta_o\cot\theta$ the total spectrum of radiation diffracted by the interferometer is summed at each point of the film upon which the diffracted beam is incident. With $|z_3|$ increasing, the ratio $\Delta\lambda/\bar{\lambda}$ decreases. Usually, $|z_3| \gg \Delta_o\cot\theta$ and $\Delta\lambda/\bar{\lambda} \ll 1$. For instance, for the reflection 220 of Si at $\Delta_o \simeq 200$ μm, $\Delta b \simeq 0$, $|z_3| = 500$ mm, $\cos\psi \simeq 1$, $\lambda \simeq 1{\cdot}54$ Å $\Delta\lambda/\bar{\lambda}$ is $1{\cdot}5 \times 10^{-3}$ (for comparison, the value of $\Delta\lambda/\lambda$ for the characteristic Cu $K\alpha_1$ line at the height $1/e$ is $0{\cdot}4 \times 10^{-3}$). This means that when $|z_3| \gg \Delta_o\cot\theta$ the functions $\sigma(x_q,\mathbf{r}_F)$, $|\chi_h|$, $|P_1(x_q,\mathbf{r}_F)|$ and $|P_2(x_q,\mathbf{r}_F)|$ may be thought of as constant within the variation range $|x_q| \lesssim \Delta_o + \Delta b\tan\theta/\cos\psi$ and may be put before the integral. Taking the

* Employment of a strongly absorbing interferometer is accounted for by the fact that with absorption decreasing (decrease of μT), the contrast of the moiré pattern becomes worse. In the case of a transparent interferometer with $\mu T < 1$, the fringe contrast for any moiré pattern is no better than 50% (Hart, 1968).

above into consideration, equation (8) can be written as follows:

$$I_h(\mathbf{r}_F) = Q(\mathbf{r}_F) \int_{-\infty}^{\infty} \exp(-x_q^2/\Delta_o^2) \times [1 + \exp(-\Delta b^2 \tan^2\theta/\Delta_o^2 \cos^2\psi) \times \cos\Phi(x_q,\mathbf{r}_F)]\,dx_q. \quad (11)^*$$

Here $Q(\mathbf{r}_F) = (c/4\pi m_x m_y)\,\sigma(0,\mathbf{r}_F)|\chi_h|^2|P_1(0,\mathbf{r}_F)|^2 \times |P_2(0,\mathbf{r}_F)|^2$ is a slowly varying function depending on the geometry of the experiment and on $\bar{\lambda}$ of the wave incident upon the observation point $\mathbf{r}_F$; $\Phi = \arg\{E_h^{\mathrm{I}}/E_h^{\mathrm{II}}\}$ is the phase difference between interfering waves.

Formula (11) gives a complete description of the polychromatic interference pattern. This pattern is defined by the parameters Δ_o, Δb and Φ, depending on the experiment geometry, the character of the interferometer deflection from the ideal one, and so on. Let us analyse equation (11), and estimate coherent properties of polychromatic beams and compare them with the coherence of the quasi-monochromatic radiation of spectral lines under the same experimental conditions, and finally derive the formulas defining the contrast of interference fringes.

2. Coherence of X-ray beams diffracted by the LLL interferometer

In optics spatial and time coherences are considered. The concept of time coherence is well illustrated by the experiment with the Michelson interferometer. A light ray radiated by the point source divides into two beams. These two beams converge again with the path difference equal to $c\Delta\tau$, where $\Delta\tau$ is the time difference between beam paths I and II. The phases of interfering waves become different and depend on the cyclic frequency of radiation $\omega(\Phi = \omega\Delta\tau)$. Provided that the radiation is not monochromatic, the interference patterns for different wavelengths are displaced with respect to one another. In order to observe the interference from this source it is required that $\Delta\omega\Delta\tau < 2\pi$; here $\Delta\omega$ is the spectral width of the radiation. The concept of spatial coherence is usually illustrated by the Young experiment, in which the two pinholes are illuminated by an extended monochromatic source. The rays from different points of the source reach the observation point following different paths, so that the interference patterns produced by different points of the source are shifted with respect to one another. The total interference pattern is observed only if these shifts are small.

In the case under consideration the interfering fields V_h^{I} and V_h^{II} at the observation point are formed, as was the case in the Michelson experiment, by summing the fields E_h^{I} and E_h^{II} from waves with different wavelengths located in the range defined by equation (10).* The rays for each wavelength trace different paths in the interferometer, as well as in the case of the Young experiment with an extended monochromatic source. It is easy to see that here the region of the width $2T\tan\varepsilon_m/|m_x|\cos\psi$ on the surface of the first wafer of the interferometer [see equations (1) and (6)] plays the role of the size of the source. Each point in this region is a source of monochromatic radiation, its wavelength being defined by equation (1) and changing from point to point. Thus, when using a point polychromatic source, the experiment under consideration with the X-ray interferometer is analogous to the Young interference experiment in which the radiation wavelength would smoothly vary from point to point of the extended source.

The analogy drawn between the above mechanisms of the interference-pattern formation and also the estimation of the range of wavelengths summing at each point of the interferogram at $|z_3| \gg \Delta_o \cot\theta$ allow one to conclude that the conditions for the polychromatic moiré-pattern formation are close to those which have been derived for the monochromatic extended source by Bonse & te-Kaat (1971).

Let us now estimate the degree of the time coherence of interfering beams. It is required that $\Delta\omega.\Delta\tau$ should be $\gtrsim 2\pi$ for the interference to vanish when summing different wavelengths (as a result of insufficient time coherence). The refractive index for X-rays differs only slightly from unity ($|\Delta n| \lesssim 10^{-5}$); therefore, in order to obtain a noticeable optical path difference between beams I and II a thick wafer should be placed in one of the beam paths. Let us estimate the wafer thickness (t_w) required for eliminating the coherence of fields V_h^{I} and V_h^{II}. Using equation (A.19), the variation range x_q for interfering waves ($|x_q| \lesssim \Delta_o - |\Delta b|\tan\theta/\cos\psi \leq \Delta_o$) and $\Delta\tau = \Delta n t_w/c\cos\psi$ we obtain $t_w \gtrsim \lambda|z_3|\tan\theta/|\Delta n|\Delta_o\cos^2\theta\cos\psi$. At $|z_3| = 500$ mm, $\Delta_o = 200$ μm, $\lambda \simeq 1{\cdot}54$ Å, $|\Delta n| \simeq 10^{-5}$, reflection 220 of Si $t_w \gtrsim 2$ cm. From this estimate it is clear that the time coherence of interfering waves in this experiment may always be assumed to be sufficient, the dependence of Φ on τ may be omitted, and the contrast of interference fringes may be considered to be caused by the degree of spatial coherence, as in the interference pattern in an X-ray interferometer formed by the

* In this equation we have taken account of the fact that $\int_{-\infty}^{\infty}\exp[-x_q \mp \Delta b\tan\theta/\cos\psi)^2/\Delta_0^2]\,dx_q$ is independent of Δb.

* Fields V_h^{I} and V_h^{II} are determined by $V_h^{\mathrm{I(II)}}(\mathbf{r}_F) = \int_{-\infty}^{\infty} E_h^{\mathrm{I(II)}}(x_q,\mathbf{r}_F)\,dx_q$.

extended monochromatic source, the effective size of such a source being equal to $2T\tan\varepsilon_m/|m_x|\cos\psi$.

To determine the contrast of interference fringes the visibility function is usually used (Born & Wolf, 1964):

$$v = (I_{\max} - I_{\min})/(I_{\max} + I_{\min}). \qquad (12)$$

Here $I_{\max}$ and $I_{\min}$ are the maximum and minimum intensities of the neighbouring extrema of the function $I_h(\mathbf{r}_F)$. At $v = 1$ the contrast of the fringes is at a maximum, but if $v = 0$, the fringes are absent.

By analysing equations (*A*.18) and (*A*.13) one can conclude that the phase difference of the interfering beams E_h^{I} and E_h^{II} is linearly dependent on the variable x_q. This property permits $\Phi(x_q,\mathbf{r}_F)$ to be represented in the form:

$$\Phi(x_q,\mathbf{r}_F) = \Phi_1(\mathbf{r}_F) + \Phi_2(\mathbf{r}_F)\,x_q, \qquad (13)$$

where $\Phi_1(\mathbf{r}_F) = \Phi(0,\mathbf{r}_F)$ and $\Phi_2(\mathbf{r}_F) = \partial\Phi(0,\mathbf{r}_F)/\partial x_q$. For instance, (see §§4 and 5), for the rotational moiré pattern $\Phi = \Phi_1 = \Lambda_\gamma^{-1} y_F$, for the dilatational moiré pattern $\Phi_1 = \Lambda_d^{-1} x_F$ and $\Phi_2 = \Lambda_d^{-1}(1 + m_x - m_x t_A/T)$, and for the interference pattern of the defocused interferometer $\Phi_2 =$ constant $\times\ \Delta b(\mathbf{r}_F)$ (here Λ's are the periods of moiré fringes).

Representation of $\Phi(x_q,\mathbf{r}_F)$ in the form of (13) permits one to obtain an analytic form for both the linear density of intensity $I_h(\mathbf{r}_F)$ and the visibility function v. Inserting equation (13) into equation (11) and using the tabulated integral (Dwight, 1961),

$$\int_{-\infty}^{\infty} \exp(-ax^2)\cos Bx\,\mathrm{d}x = (\pi/a)^{1/2}\exp(-B^2/4a),$$

we obtain

$$I_h(\mathbf{r}_F) = Q'(\mathbf{r}_F)[1 + \exp(-\zeta^2)\cos\Phi_1(\mathbf{r}_F)], \qquad (14)$$

where $Q'(\mathbf{r}_F) = \pi^{1/2}\Delta_o Q(\mathbf{r}_F)$ and $\zeta^2 = (\Delta b\tan\theta/\Delta_o\cos\psi)^2 + (\Delta_o\Phi_2/2)^2$. The equation obtained describes the intensity distribution in the interferogram for the majority of experimental situations. The function $Q'(\mathbf{r}_F)$ defines the general form of the distribution $I_h(\mathbf{r}_F)$. Variation of function $\Phi_1(\mathbf{r}_F)$ leads to the appearance of polychromatic moiré fringes, the distances between them being determined by the condition $\Phi_1(\mathbf{r}_F'') - \Phi_1(\mathbf{r}_F') = 2\pi N$ ($N = 1, 2, 3, \ldots$).

It follows from equations (12) and (14) that the visibility function has the form

$$v = \exp(-\zeta^2). \qquad (15)$$

It can be seen from equation (15) that the visibility of polychromatic interference fringes depends on the parameter ζ. With ζ increasing the contrast of the fringes rapidly deteriorates. Condition $\zeta \lesssim 1{\cdot}5$ may serve as a criterion for observing the moiré pattern (at $\zeta = 1{\cdot}5$, $v \simeq 0{\cdot}1$).

The problem considered is similar to that of the interference-pattern formation when using a monochromatic source extended along the **OX** direction. In this case, on the assumption that the intensity of the source radiation $\rho(x_f)$ does not in practice change at distances of the order of $2\Delta_o$, the interference pattern on the film is also described by equations (14) and (15), where $Q(\mathbf{r}_F) = (c/4\pi m_y)|\chi_h|^2|P_1|^2|P_2|^2\rho(x_F - z_3\tan\theta/\cos\psi)$ and $x_q = x_F - x_f - z_3\tan\theta/\cos\psi$. It should be noted that the expression obtained for the visibility function (15) differs from that derived by Bonse & te-Kaat (1971) for an extended monochromatic source on the assumption that E_h^{I} and E_h^{II} are constant in the range $|x_q \mp \Delta b\tan\theta/\cos\psi| \le T\tan\varepsilon_m/\cos\psi$ and are zero outside it. A comparison between the theoretical and experimental results of Bonse & te-Kaat relating to the fringe contrast of the defocused interferometer and the theoretical results obtained in the present work are discussed in §4.

Let us consider examples of the application of the above equations for the analysis of a polychromatic moiré pattern and find the view of the interference patterns for the case when all the deflections of the interferometer from the ideal one refer to the A wafer only.

3. Moiré pattern of a focused interferometer

In the case of a focused interferometer $\Delta b = 0$, and, therefore [see equations (*A*.18) and (14)]:

$$\Phi(x_q,\mathbf{r}_F) = \arg\{\chi_h/\chi_{hA}\} + (\varphi^{\mathrm{I}} - \varphi^{\mathrm{II}}),$$
$$\zeta^2 = 0{\cdot}25\,\Delta_o^2[\partial\Phi(0,\mathbf{r}_F)/\partial x_q]^2. \qquad (16)$$

Here χ_h corresponds to the first two wafers of the interferometer, χ_{hA} to the last. The value of $\varphi^{\mathrm{I}} - \varphi^{\mathrm{II}}$ is defined by variation of the conditions of the Bragg reflection in wafer A for the fields E_h^{I} and E_h^{II} [see equations (*A*.13) and (*A*.14)]. In a focused interferometer the moiré-fringe spacings and their contrast depend on $\arg\{E_h^{\mathrm{I}}/E_h^{\mathrm{II}}\} = \Phi(x_q,\mathbf{r}_F)$ only. Below, the connection between the main type of interferometer deflection from the ideal one and the moiré patterns observed is determined, and the moiré-fringe spacings Λ and their visibility v are calculated.

(*a*) *Translational moiré pattern*

Suppose wafer A is displaced as a whole for a distance $\Delta\mathbf{r}$. At such a displacement the structure amplitude of reflection, and, consequently, the value of χ_{hA}, vary by the phase factor $\exp[-i(\mathbf{h}\Delta\mathbf{r})]$, where $\mathbf{h}$ is the vector of the reciprocal lattice ($h = 2\pi/d_h$). Conditions of the Bragg reflection in wafer A do not vary and $\Phi = (\mathbf{h}\Delta\mathbf{r})$. This means that in displacing the analyser (wafer A) in the direction of the reciprocal-

lattice vector for the given reflection, the intensity $I_h(\mathbf{r}_F)$ for any observation point $\mathbf{r}_F$ oscillates with the period:

$$\Lambda_{tr} = d_h. \tag{17}$$

For a translational moiré pattern, Φ is independent of x_q and $\mathbf{r}_F$, therefore $v_{tr} = 1$ even at the point where the polychromatic beams focus, q.

(*b*) *Rotational moiré pattern*

Let us turn the analyser by a certain angle γ with respect to the axis parallel to the normal to the interferometer wafers. Once $\gamma \ll 1$, then χ_{hA} changes by the factor $\exp\{i[(\Delta\mathbf{hr}_{A2}) + \varphi_o]\} = \exp[i(h\gamma y_{A2} + \varphi_o)]$ (here phase φ_o is related to the position of the rotation axis relative to the interferometer). Angular parameters α^{I} and α^{II} for both interfering fields remain equal and $\varphi_I = \varphi^{II}$ [see equations (*A*.14) and (*A*.13)]. Thus, using equation (4), we obtain $\Phi = -h\gamma m_y^{-1} y_F + \varphi_o$. On the film there may be observed the fringes in parallel with the **OX** direction with the spacing Λ_γ:

$$\Lambda_\gamma = m_y d_h/\gamma. \tag{18}$$

For the rotational moiré pattern, as well as for the translational one, the focused interferometer is an achromatic device as Φ is independent of x_q. So, v_γ is equal to 1 at any point $\mathbf{r}_F$.

(*c*) *Dilatational moiré pattern*

Suppose the lattice spacing of the analyser differs by a quantity Δd_h from that of the rest of the wafers of the interferometer. Then $\arg\{\chi_h/\chi_{hA}\} = -(\Delta\mathbf{hr}_{A2}) + \varphi_o$ (here phase φ_o is related to the 'origin' of deformation), and $\varphi^{I} - \varphi^{II} = (\Delta h t_A/T)(x_{A2} + z_1 \tan\theta + T\tan\theta)$ [see equations (*A*.14) and (*A*.13)]. Replacing $\mathbf{r}_{A2}$ by $\mathbf{r}_F$ and using equations (4) and (6) we obtain $\Phi \sim -(\Delta d_h/d_h^2) m_x^{-1}[x_F - (1 + m_x - m_x t_A/T)x_q] + \varphi_o$. On the film there appear moiré fringes parallel to the **OY** direction. The spacing of these fringes, Λ_d, is determined by the coefficient before x_F and is:*

$$\Lambda_d = |m_x| d_h^2/|\Delta d_h|. \tag{19}$$

The visibility of dilatational moiré fringes depends on the coefficient before x_q and is [see equation (15)]:

$$v_d = \exp\{-[(1 + m_x - m_x t_A/T)\Delta_o/2\Lambda_d]^2\}. \tag{20}$$

From equation (20) it follows that the moiré pattern is seen under the condition: $\Lambda_d > 0{\cdot}33(1 + m_x - m_x t_A/T)\Delta_o$. This condition limits the value of Δd_h. At $m_x = 1$, $\Delta_o = 200$ μm, $t_A/T = 1/3$ $\Delta d_h/d_h < 1{\cdot}8\, d_h/\Delta_o \simeq 2 \times 10^{-6}$.

* The spacing of dilatational fringes in interferograms obtained with a point polychromatic source at $|m_x| = 1$ coincides with that obtained with a monochromatic source extended in the **OX** direction.

(*d*) *Interference pattern of the phase-shifting object*

Let us put a thin plane-parallel wafer of thickness t_w in one of the interferometer beams parallel to the interferometer crystals. This wafer introduces the phase difference $\Phi = \pi\chi_o t_w/\lambda\cos\theta\cos\psi = 2\pi\chi_o t_w d_h(x_F - x_q)/\lambda^2 z_3$ between the interfering waves E_h^{I} and E_h^{II}. On the film there appear moiré fringes parallel to the **OY** direction with the spacing:*

$$\Lambda_w = |m_x| z_1 \lambda^2/\chi_o t_w d_h. \tag{21}$$

As in § 3(*c*), Φ depends on $x_q(\Phi_2 = \Lambda_w^{-1})$ and

$$v_w = \exp[-(\Delta_o/2\Lambda_w)^2]. \tag{22}$$

The condition for observing the moiré fringes caused by the phase-shifting object is $\Lambda_w > 0{\cdot}33\Delta_o$. Note that the thickness of this object should not exceed that which introduces a larger optical path difference than the coherence length of the diffracted radiation monochromatized by the interferometer.

Let us compare the results obtained $\{\Lambda_{tr} = d_h$, $v_{tr} = 1$; $\Lambda_\gamma = m_y d_h/\gamma$, $v_\gamma = 1$; $\Lambda_d = |m_x| d_h^2/|\Delta d_h|$, $v_d = \exp[-(1 + m_x - m_x t_A/T)^2\Delta_o^2/4\Lambda_d^2]$; and $\Lambda_w = |m_x| z_1\lambda^2/|\chi_o| d_h t_w$, $v_w = \exp[-(\Delta_o/2\Delta_w)^2]\}$ with those known for the case of monochromatic plane waves. As follows from the theory of electron-microscopic moiré patterns (Gevers, 1962), the fringe spacings and the fringe visibilities for the main moiré types are defined by the following expressions: $\Lambda_{tr} = d_h$, $v_{tr} = 1$; $\Lambda_\gamma = d_h/\gamma$, $v_\gamma = 1$; $\Lambda_d = d_h^2/|\Delta d_h|$, $v_d = 1$; and $\Lambda_w = \infty$, $v_w = 0$. The fringe spacings for rotational and dilatational moiré patterns for the case of plane waves differ from the corresponding expressions for the polychromatic moiré pattern owing to the divergence of polychromatic diffracted beams in both the **OX** and **OY** directions. The difference between the dilatational moiré pattern visibilities is because in the case of polychromatic radiation the different wavelengths are summed at the observation point with different phase relations between the interfering waves. A variation in the wavelength in the **OX** direction leads to the appearance of moiré fringes caused by a phase-shifting object even if it is a plane-parallel wafer.

Thus, in a number of cases the fringe spacings and the fringe visibilities of the X-ray polychromatic moiré pattern differ from those of the monochromatic moiré pattern in plane waves and are dependent on both the misalignment type and the experimental geometry.†

* In the case of a monochromatic source fringes will appear on the film parallel to the **OX** direction; these are due to a change in the angle ψ with a change in diffraction planes and in the case of monochromatic plane waves $\Lambda_w = \infty$.

† There is a more general statement in Shulakov & Aristov (1978) on the dependence of the fringe spacing and fringe visibility of an X-ray moiré pattern on the type of misalignment, the experimental geometry, the source size and the spectral composition of the radiation.

The problem concerning the effect of defocusing on the moiré pattern is of importance for an experimental observation on a polychromatic moiré pattern; §4 deals with this problem.

4. Interferometer with distorted focusing

We have already mentioned that there is an analogy between summing the intensities of the waves radiated by a polychromatic point source and in summing those radiated by a monochromatic extended source. As was shown by Bonse & te-Kaat (1971), in the defocused interferometer the contrast of interference fringes fades mainly because the rays incident at an observation point from different source points have different phase relations between interfering waves.

The same thing occurs in the present case, since the phase relations between the interfering waves $E_h^{\rm I}(\lambda,\mathbf{r}_F)$ and $E_h^{\rm II}(\lambda,\mathbf{r}_F)$ are different for the different wavelengths. The phase difference Φ for the defocused interferometer is always dependent on x_q, even in the absence of other misalignments. This circumstance gives rise to fading contrast of the fringes. In particular, for the translational and rotational moiré patterns and for the defocused pattern caused by a change of Δb the parameter Φ_2 does not equal zero, and the visibility function is determined by [see equations (14) and (15)]:

$$v = \exp[-(\eta/2)^2 - (\Delta b \tan\theta/\Delta_o \cos\psi)^2], \quad (23)$$

where $\eta = \Phi_2\Delta_o = (2\pi\Delta b\Delta_o/l_oT\tan\theta)$ and $l_o = \lambda\cos\theta/|\chi|$ is the extinction distance. The term $\Delta b\tan\theta/\Delta_o\cos\psi$ in equation (23) appears to result from the fact that at $\Delta b \neq 0$ the interfering wavefields overlap only partially. This overlap and, consequently, the wavefield coherence vanish at $|\Delta b| \gtrsim \Delta_o\cos\psi/\tan\theta$. If the fringe visibility should be determined by overlap of beams $E_h^{\rm I}(\lambda,\mathbf{r}_F)$ and $E_h^{\rm II}(\lambda,\mathbf{r}_F)$ only, then for the example considered the defocus value could reach 440 μm (this case corresponds to the experiment with a point monochromatic source). The effect of the parameter η turns out to be more important, since for any defocus $\Delta b\tan\theta/\Delta_o\cos\psi = \eta|\chi''|/2|\chi| \ll \eta$, and the visibility function (23) has the form:

$$v = \exp\left[-\frac{\eta^2}{4}\left(1 + \left|\frac{\chi''}{\chi}\right|^2\right)\right]. \quad (24)$$

The approximate expression of equation (24) is $v = \exp(-\eta^2/4)$.

From equation (24) it follows that the fringe visibility decreases by e times at

$$|\Delta b| \simeq l_oT\tan\theta/\pi\Delta_o. \quad (25)$$

Condition (25) defines the requirements for the accuracy of interferometer manufacturing. For instance, for the interferometer considered and the wavelength $\lambda \simeq 1{\cdot}54$ Å the accuracy of manufacturing should be such that $|\Delta b| \lesssim 17$ μm. At larger values of $|\Delta b|$ the interference pattern is not observed in practice.

It has been noted above (§2) that the expression for the visibility function (15) of polychromatic fringes is also valid for the case of an extended monochromatic source. Therefore, it is of interest to compare the dependence of $v(\Delta b)$ with the theoretical and experimental results of Bonse & te-Kaat (1971). In the theory developed by them it was assumed that the intensity distribution of a coherent wavefield on the exit interferometer surface has the form $\theta'(T\tan\varepsilon_m - |x_q|)$ (here θ' is the Heaviside step function being equal to unity at a positive value of the argument and to zero at a negative value; x_q is the distance between the observation point $\mathbf{r}_F$ and the centre of the coherent wavefield). In this approximation, the visibility function is described by

$$v'(\Delta b) = \frac{|\sin[\eta'(1 - \Delta b\tan\theta/T\tan\varepsilon_m)]|}{\eta'}, \quad (26)$$

where $\eta' = 2\pi\Delta b\tan\varepsilon_m/l_o\tan\theta$. A comparison between $v(\Delta b)$ and $v'(\Delta b)$ shows that the visibility function is markedly dependent on the form of the distribution $|E_h^{\rm I(II)}(x_q,r_F)|$. This difference is especially evident at large values of the parameters η and η'. It is known that in the case of weak absorption ($\mu T < 1$) the intensity distribution on the exit surface of a crystal is a complicated oscillating function of x_q. At $\mu T \gtrsim 5$ the oscillations practically disappear, and at $\mu T \gtrsim 40$ the distribution $|E_h^{\rm I(II)}(x_q,\mathbf{r}_F)|^2$ is well described by the Gaussian function [see equation (A.17)]. It follows from the above that expression (24) is precise at large μT, and it describes the fringe visibility with a certain approximation at $5 \lesssim \mu T \lesssim 40$. The approximation used by Bonse & te-Kaat is less precise at any μT and can, therefore, be used for the estimation of the interference-pattern visibility at small values of the parameter η' only (at $\eta' \lesssim \pi/2$).* Thus, for instance, expression (26) predicts the presence of the visibility-function oscillations with an increase of η'. As can be seen from (24) this effect is a result of the approximation used and cannot be observed in the experiment (at least, at $\mu T \gtrsim 5$).

Fig. 3 represents the theoretical curves $v(\Delta b)$ and $v'(\Delta b)$ and the experimental data by Bonse & te-Kaat (1971) obtained for a silicon LLL interferometer with $T = 831$ μm ($\mu T \simeq 12{\cdot}7$), for Cu $K\alpha$ radiation, the 220 reflection and $\cos\psi \simeq 1$. It can be seen that at large values of η' the experimental points are closer to dependence $v(\Delta b)$ (curve 1) than to dependence $v'(\Delta b)$ (curve 2). The second and subsequent maxima of $v'(\Delta b)$

* This estimation is obtained from the Rayleigh criterion and the relation: $\arg\{E_h^{\rm I}(-T\tan\varepsilon_m,\mathbf{r}_F)/E_h^{\rm II}(T\tan\varepsilon_m,\mathbf{r}_F)\} = \eta'$.

are not experimentally observed, in accordance with function (24).

Thus, a polychromatic interference pattern should be observed under the same conditions as in the case of a monochromatic extended source, and the requirements for the accuracy of interferometer manufacturing are not very strict.

So far, the term 'point source' has been used by us in a mathematical sense. A physical source has real physical dimensions. Evidently, when using an extended polychromatic source the interference pattern becomes diffuse and when the source dimensions are large enough, it will vanish. In the next section, an effect of the source extension on the fringe contrast will be considered, and the requirements for source dimensions at which the pattern observed does not markedly change will be established.

5. Influence of source dimensions on the fringe contrast

We shall now determine the intensity distribution formed on a film in the case of an incoherent extended polychromatic source. Let $\rho(\mathbf{r}_f)$ describe the source luminosity at a point $\mathbf{r}_f$, and isolate in the vicinity of $\mathbf{r}_f$ a small volume whose dimensions are much less than Δ_o. On the film this quasi-point source will be accounted for by an intensity distribution $dI_h^{\text{e.s.}}(\mathbf{r}_f,\mathbf{r}_F) = \rho(\mathbf{r}_f) I_h^{\text{p.s.}}(\mathbf{r}_f,\mathbf{r}_F) dv_f$, where $I_h^{\text{p.s.}}$ is $I_h(\mathbf{r}_F - \mathbf{r}_f)$ and is determined by equation (14) (here the abbreviations e.s. and p.s. are extended source and point source, respectively). The total intensity distribution produced by all the quasi-point sources is given by the convolution of the functions $\rho(\mathbf{r}_f)$ and $I_h(\mathbf{r}_F - \mathbf{r}_f)$:

$$I_h^{\text{e.s.}}(\mathbf{r}_F) = \int_{v_f} \rho(\mathbf{r}_f) Q'(\mathbf{r}_F - \mathbf{r}_f) \{1 + \exp[-\zeta^2(\mathbf{r}_F - \mathbf{r}_f)] \times \cos \Phi_1(\mathbf{r}_F - \mathbf{r}_f)\} dv_f. \quad (27)$$

The functions $Q'(\mathbf{r}_F - \mathbf{r}_f)$ and $\zeta(\mathbf{r}_F - \mathbf{r}_f)$ are determined in equations (11) and (14). As the experimental geometry is invariable, these functions are dependent on the wavelength $\bar{\lambda}$, defined by the relation [see equation (6)]:

$$\tan\theta = (x_F - x_f)\cos\psi / z_3. \quad (28)$$

It follows from equation (28) that in the case of an extended polychromatic source $\bar{\lambda}$ depends on a change of the coordinates of the point $\mathbf{r}_f\{\psi = \arctan[(y_F - y_f)/(z_F - z_f)]\}$. Consider the source with $\rho(\mathbf{r}_f) = \rho_o \theta'(f_x - |x_f|)\theta'(f_y - |y_f|)\delta(z_f)$ (here δ is the Dirac function). The variation range of $\bar{\lambda}$ for this source is

$$\Delta\bar{\lambda}/\bar{\bar{\lambda}} \simeq (2f_x \cos^2\theta \cos\psi/|z_3|\tan\theta) + (2^{1/2} f_y \cos\theta / z_F)^2, \quad (29)$$

where $\bar{\bar{\lambda}}$ is determined by equation (28) at $\mathbf{r}_f = 0$. Under the conditions

$$2f_x \ll |z_3| \tan\theta / \cos^2\theta \cos\psi$$

and

$$2f_y \ll 2^{1/2} z_F / \cos\theta, \quad (30)$$

the ratio $\Delta\bar{\lambda}/\bar{\bar{\lambda}} \ll 1$, and the functions $Q'(\mathbf{r}_F - \mathbf{r}_f)$ and $\zeta(\mathbf{r}_F - \mathbf{r}_f)$ can be considered as constant within the variation range of $\mathbf{r}_f$ and assumed to be equal to $Q'(\mathbf{r}_F)$ and $\zeta(\mathbf{r}_F)$ respectively. Above, the ratio $\Delta\bar{\lambda}/\bar{\lambda}$ has been estimated for the wavelengths summing at the observation point in the case of a polychromatic point source. It turned out that $\Delta\bar{\lambda}/\bar{\lambda} \simeq 1{\cdot}5 \times 10^{-3}$. The same magnitude for the ratio $\Delta\bar{\lambda}/\bar{\bar{\lambda}}$ corresponds to an extended source with the dimensions $2f_x \simeq 200$ μm and $2f_y \simeq 20$ mm (at $z_1 \simeq -z_3 \simeq 500$ mm, $\bar{\lambda} \simeq 1{\cdot}54$ Å and $\cos\psi \simeq 1$). So, the conditions (30) hold for the majority of X-ray fine-focus sources.

If the conditions (30) are satisfied and the first derivatives of $\Phi_1(\mathbf{r}_F - \mathbf{r}_f)$ change only insignificantly at distances of the order of f_x and f_y, the phase difference $\Phi_1(\mathbf{r}_F - \mathbf{r}_f)$ in the first approximation can be represented as

$$\Phi_1(\mathbf{r}_F - \mathbf{r}_f) \simeq \Phi_1(\mathbf{r}_F) + \Phi_{11}(\mathbf{r}_F) x_f + \Phi_{12}(\mathbf{r}_F) y_f, \quad (31)$$

where $|\Phi_{11}(\mathbf{r}_F)| = 2\pi(m_x + 1)\Lambda_x^{-1}$ and $|\Phi_{12}(\mathbf{r}_F)| = 2\pi(m_y - 1)\Lambda_y^{-1}$. The representation $\Phi_1(\mathbf{r}_F - \mathbf{r}_f)$ in the

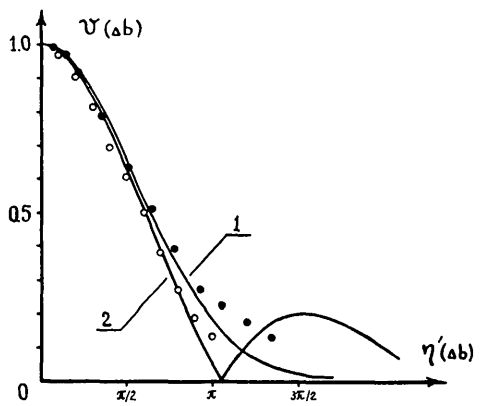

Fig. 3. Theoretical and experimental dependences of the fringe visibility as a function of a defocusing Δb. Curves (1) and (2) correspond to the expressions (24) and (26) respectively. For the points denoted by dark circles the value of $\tan\varepsilon_m$, measured experimentally, is 0·116; for the points denoted by light circles $(\tan\varepsilon_m)_{\text{exp}} = 0{\cdot}136$. The axis of Δb (axis of abscissa) is given in units of η'. The value of Δ_o in (24) was assumed to equal $T(\tan\varepsilon_m)_{\text{exp}}/(\ln 2)^{1/2}$.

form of (31) permits one to obtain an analytic form of the visibility function:

$$v^{\text{e.s.}} = \exp(-\zeta^2)\frac{|\sin[2\pi(m_x+1)\Lambda_x^{-1}f_x]|}{2\pi(m_x+1)\Lambda_x^{-1}f_x} \times \frac{|\sin[2\pi(m_y-1)\Lambda_y^{-1}f_j]|}{2\pi(m_y-1)\Lambda_y^{-1}f_y}. \quad (32)$$

Thus, for the moiré patterns with constant fringe spacing (see § 3) and also for those in which the fringe spacing is a slowly varying function of coordinates, the fringe visibility depends on the source dimensions as $|\text{sinc}\,[2\pi(1+z_3/z_1)\Lambda^{-1}f]|$.* This means that only those fringes are observed for which $\Lambda_x > 2f_x(m_x+1)$ and $\Lambda_y > 2f_y(m_y-1)$. For the fringes with spacings $\Lambda_x \gg 2f_x(m_x+1)$ and $\Lambda_y \gg 2f_y(m_y-1)$, an extended source with dimensions $2f_x$ and $2f_y$ satisfying the conditions (30) can be considered as a point one.

So, on the base of the above, it can be concluded that moiré patterns can be observed with polychromatic radiation. To verify this conclusion, an experiment was carried out, the results of which are presented in § 6.

6. Experimental results

A symmetric LLL interferometer with 220 reflecting planes has been made from a Si single crystal. Its characteristics are: $b_1 \simeq b_2 \simeq 10$ mm, $t_S \simeq t_M \simeq t_A \simeq 0{\cdot}8$ mm, $T \simeq 2{\cdot}4$ mm, $|\Delta b| \lesssim 20$ μm. The experiment was carried out with a 'Microflex' microfocusing X-ray generator. The radiation of a gold anode in the range of wavelengths 1·2–1·4 Å was used; the focus diameter did not exceed 20 μm. In the range of wavelengths 1·2–1·4 Å, $\Delta_o \simeq 270$–250 μm, $2\pi|\chi''|T/\lambda\cos\theta \simeq 17$–$27$, $(\tan\theta/\tan\varepsilon_m)^2 \gtrsim 10$. Thus, all the results obtained above may be applied to this interferometer.

The geometry of the experiment was in accordance with Fig. 1 ($z_1 = 100$–150 mm, $z_3 = 50$–300 mm) and was very similar to that of Aristov, Shmytko & Shulakov (1977*b*). In order to decrease the background of radiation scattered by various elements of the experimental scheme the primary beam divergence was limited to 4–6° by slit 1. In the vicinity of the points q ($x = 0$, $z_3 = 0$) the beams $E_{ohh} + E_{hoh}$ ($E_h^{\text{I}} + E_h^{\text{II}}$ in the other designation) of different wavelengths are focused in the narrow band about $2\Delta_o$ wide parallel to the **OY** direction. Slit 2 placed in the location of the focal band fully transmitted the beam $E_{ohh} + E_{hoh}$ (the slit width was 1 mm) and protected the film from the beams E_{ooh} and E_{hhh} (these beams are not shown in Figs. 1 and 2) and the primary beam.* Besides, slit 2 permits a considerable diminution of the level of the incoherent background of the primary radiation scattering by the S, M and A wafers of the interferometer.

Fig. 4 shows a photograph of the pattern obtained in the scheme of Fig. 1 without slit 2, $z_1 \simeq z_3 \simeq 100$ mm. The photograph distinctly exhibits the beams E_{ooh}, $E_{ohh} + E_{hoh}$ and E_{hhh} corresponding to diffraction of the characteristic Au $L\alpha$ radiation ($\lambda \simeq 1{\cdot}28$ Å). The spacing of moiré fringes in the beam $E_{ohh} + E_{hoh}$ is 0·5–4 mm. Alongside the line of characteristic radiation, the diffraction background is also visible; it is caused by scattering of the polychromatic spectrum in all the wafers of the interferometer.

Having set up slit 2 for removing the diffracted beams E_{ooh} and E_{hhh}, and after exposing for an ex-

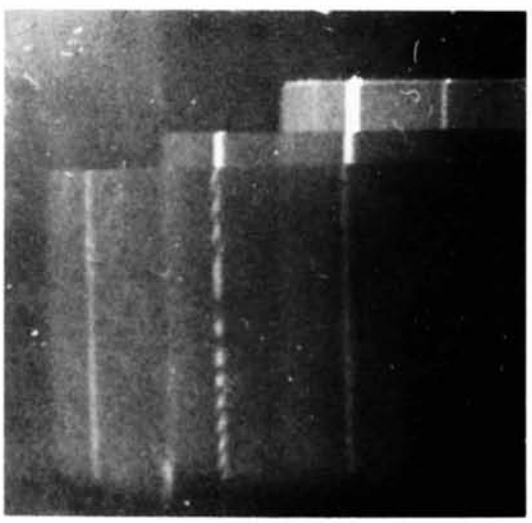

Fig. 4. Topographic image produced by the LLL interferometer with an X-ray divergent polychromatic beam. Images of S, M and A wafers of the interferometer are formed by the continuous spectrum. The light lines are related to the characteristic radiation Au $L\alpha$ ($\lambda \simeq 1{\cdot}28$ Å) and correspond to the diffracted beams: E_h on the S wafer, E_{oh} and E_{hh} on the M wafer, E_{ooh}, $E_{ohh} + E_{hoh}$ and E_{hhh} on the A wafer (the second weak line on the S wafer corresponds to Au $L\eta$ radiation with $\lambda \simeq 1{\cdot}4$ Å). The beam $E_{ohh} + E_{hoh}$ depicts interference between the wavefields I and II. The slight shifts between the beams E_h, E_{hh} and E_{hhh} and also between E_{oh} and $E_{ohh} + E_{hoh}$ are due to the narrowing of wavefield angular width in the interferometer wafers.

* An analogous expression can be obtained for an extended quasi-monochromatic source. In this case, the parameter f will act as a spectral radiation width.

* In practice, for any LLL interferometer, slit 2 can be used to separate the beam $E_{ohh} + E_{hoh}$ from the beams E_{ooh} and E_{hhh}. This is because beams E_{ooh} and E_{hhh} are focused in other planes with z = constant ($z = 2z_1 + 2z_L$ and $z = 2z_1 + t_s$) and under the condition $z_L \tan\theta_{\min} > \Delta_o$ they do not overlap with beam $E_{ohh} + E_{hoh}$ in the region of slit 2. This is impossible for beams E_{ooo}, $E_{oho} + E_{hoo}$ and E_{hho} and thus they have no focusing points.

tended time we succeeded in obtaining a moiré pattern with polychromatic radiation in the wavelength range 1·2–1·4 Å. The photograph of the moiré pattern obtained is shown in Fig. 5. The polychromatic moiré fringes are almost parallel to the interferometer foot and intersect the moiré pattern on the line of characteristic radiation at the maximum intensity points. When the distance z_3 was changed the fringe spacing varied in accord with a change of the geometrical magnification coefficients m_x and m_y. The fringe contrast is smeared, since the interferometer is defocused (at $|\Delta b| \simeq 20$ μm, $v \simeq 0{\cdot}37$) and slit 2 does not permit one to eliminate completely the incoherent background caused by the primary X-ray beam scattering by the interferometer wafers (this mainly refers to wafer M).

Thus, the experiment shows that interference patterns can also be observed with continuous X-radiation. This is because an X-ray LLL interferometer is a special device in which the coherence of the interfering beams is mainly determined by the parameters of the experimental scheme and the device itself, and less importantly by the characteristics of tne radiation employed.

Conclusion

The X-ray interferometer has been shown to permit an interference pattern to be obtained with polychromatic radiation. Under the condition $|z_3| \gg T$, the visibility of an interference pattern does not depend essentially on the spectral composition of the radiation, and if the physical dimensions of the point source are small as compared with the spacing of the fringes observed, the fringe contrast is determined by the same parameters as in the case of an extended monochromatic source. The spacing of polychromatic fringes for a number of cases differs from those of optical and electron-microscopic moiré patterns and the X-ray moiré pattern with monochromatic radiation due to the divergence of diffracted beams in both the **OX** and **OY** directions.

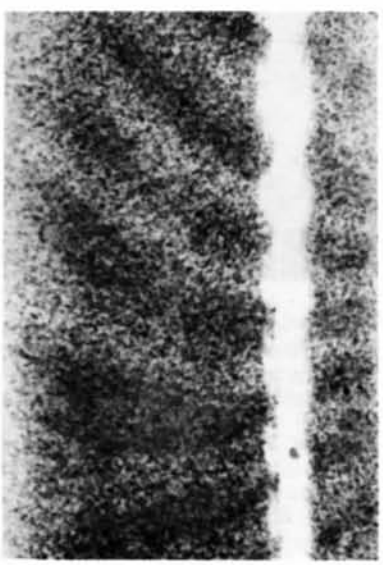

Fig. 5. Polychromatic moiré pattern of the interferometer. The overexposed light line corresponds to Au $L\alpha$ radiation.

The theory developed in this paper may be applied to the analysis of the operation of the LLL interferometer at any spectral composition of radiation, including quasi-monochromatic radiation of spectral lines. In the last case $\sigma(\lambda)$ is a rapidly varying function and cannot be put before the integral in equation (8). The shape of the spectral lines of the non-laser radiation is sufficiently well described by the Gaussian function. This means that while the point source of quasi-monochromatic radiation is used the intensity distribution in the interferogram and the visibility of interference fringes are described by equations (11), (14) and (15), as is the case with polychromatic radiation, provided parameter Δ_o is substituted by Δ_o^* in all expressions except $\Delta b \tan\theta/\Delta_o \cos\psi$ describing beam overlapping. This parameter is connected with Δ_o and with the spectral width of the characteristic radiation $\Delta\lambda/\bar{\lambda}$ by the following expression: $\Delta_o^* = \Delta_o\Delta_\lambda(\Delta_o^2 + \Delta_\lambda^2)^{-1/2}$, where $\Delta_\lambda \simeq (\Delta\lambda/\bar{\lambda})(|z_3| \tan\theta/\cos^2\theta)$. Inserting values $\Delta\lambda/\lambda$, θ and Δ_o for the 220 Si reflection of the Cu $K\alpha$ radiation and assuming $|z_3|$ to be 500 mm, we obtain $\Delta_o^* \simeq 65$ μm ($\Delta_o \simeq 200$ μm).

It is to be supposed that for some cases the interferometry scheme with polychromatic radiation may turn out to be more advantageous than those with a quasi-monochromatic source. For instance, the scheme of a translational moiré pattern is more 'apertured' on using a wide spectrum of radiation; it is also of interest to employ polychromatic radiation for determining the dependence of the crystal refractive index for X-rays on the wavelength near the absorption edges of the element and, also, for developing an X-ray phase-contrast microscope with a geometrical magnification and resolution to 1 μm (Aristov, 1978) on the basis of an LLL interferometer.

APPENDIX *A*

Diffraction of a monochromatic wave in an absorbing LLL interferometer

The wavefield at a distance r from the point source of non-monochromatic radiation may be represented as a packet of monochromatic spherical waves, $E^i(\lambda,r)$:

$$E^i(\lambda,r) = \frac{a^i(\lambda)}{4\pi r}\exp[i(kr - \omega\tau)]. \qquad (A.1)$$

Here $a^i(\lambda)$ is the Fourier component of expansion of the ith elementary act of radiation of monochromatic waves; k is the modulus of the wave vector equal to $2\pi/\lambda$; ω is the cyclic frequency; and τ is the time (in what follows the time dependence is omitted).

Let us calculate the field resulting from diffraction of each of the monochromatic waves $E^i(\lambda,r)$ in a symmetric strongly absorbing interferometer of the LLL type (see Fig. 2).

The generalized dynamical theory of X-ray scattering by perfect crystals based on Takagi's (1962) equations is used in an analysis of diffraction of the waves $E^i(\lambda,r)$ in the interferometer. According to this theory (see, for instance, Indenbom & Chukhovsky, 1972) in a two-wave approximation the space-inhomogeneous field $E(\lambda,\mathbf{r})$ in the crystal may be represented as two packets propagating in the direction of the incident (index o) and diffracted (index h) waves:

$$E(\lambda,\mathbf{r}) \simeq E_o(\lambda,\mathbf{r})\,e^{i(\mathbf{k}_o\mathbf{r})} + E_h(\lambda,\mathbf{r})\,e^{i(\mathbf{k}_h\mathbf{r})}, \qquad (A.2)$$

where $|\mathbf{k}_o| = 2\pi/\lambda$, $\mathbf{k}_h = \mathbf{k}_o + \mathbf{h}$, and $E_o(\lambda,\mathbf{r})$ and $E_h(\lambda,\mathbf{r})$ are slowly varying functions of the coordinates which are defined by the influence of the fields E_j at the points $\mathbf{r}'$ upon the field E_i at the point $\mathbf{r}$:

$$E_i(\lambda,\mathbf{r}) = \int_C G_{ij}(\lambda,\mathbf{r}-\mathbf{r}')\;E_j(\lambda,\mathbf{r}')\,d\mathbf{r}'. \qquad (A.3)$$

Here $i,j = o, h$; G_{ij} is the influence function obtained by Slobodetsky, Chukhovsky & Indenbom (1968) and Authier & Simon (1968); the vector $\mathbf{r}-\mathbf{r}'$ is in the reflection plane; and integration proceeds along the contour C restricted by characteristics of the Takagi equations.

In the case of strong absorption at $2\pi|\chi''|T/\lambda\cos\theta \gg 1$, the asymptotic expression for the influence function is:*

$$G_{oo} \simeq G_{hh} \simeq -\chi G,$$
$$G_{ho} \simeq \chi_h G \text{ and } G_{oh} \simeq \chi_{\bar{h}} G, \qquad (A.4)$$

where

$$G(\lambda,\mathbf{r}-\mathbf{r}') = P_1\left(\lambda,\frac{z-z'}{\cos\psi}\right)\exp\left\{-i\,\frac{k(x-x')}{4\sin\theta}\times\left[\alpha+\frac{(x-x')\chi\cos\psi}{(z-z')\tan\theta}\right]\right\} \qquad (A.5a)$$

and

$$P_1\left(\lambda,\frac{z-z'}{\cos\psi}\right) = \frac{1}{4}\left[\frac{k\cos\theta\cos\psi}{\pi\chi\sin^2\theta(z-z')}\right]^{1/2}\exp(i\pi/4)\times\exp\left[-i\,\frac{k(z-z')(\alpha+2\chi_o-2\chi_h)}{4\cos\theta\cos\psi}\right]. \qquad (A.5b)$$

Here $\chi = \chi' + i\chi'' = (\chi_h\chi_{\bar{h}})^{1/2}$, $\chi'' < 0$; $\alpha = (k_h^2 - k_o^2)/k_o^2$ is the angular parameter equal to $2\Delta\theta\sin 2\theta$, where $\Delta\theta$ is the deviation from the Bragg angle θ; $\psi = \arctan[(y-y')/(z-z')]$ is the angle between the diffraction plane and the plane $y-y'=0$; and $P_1(\lambda,t/\cos\psi)$ is the slowly varying function of λ ($t = z - z'$ is the crystal thickness). It follows from equation (*A*.5*a*) that $|G(\lambda;x-x',t/\cos\psi)|^2 = |P_1(\lambda,t/\cos\psi)|^2 \times \exp[-(x-x')^2/\Delta_o^2(t)]$, where $\Delta_o(t) = [\lambda t\sin^2\theta/\pi|\chi''|\cos\theta\cos\psi]^{1/2}$. Further, without digressing from the general character of the formulation, we assume that $\cos\psi = 1$ and introduce G_o for the function G with $\alpha = 0$: $G(\lambda,\mathbf{r}-\mathbf{r}')|_{\alpha=0} = G_o(\mathbf{r}-\mathbf{r}')$.

Suppose the spherical wave $E^i(\lambda,r)$ excites a space-inhomogeneous field (*A*.2) with $\alpha = 0$, $|\mathbf{k}_o| = |\mathbf{k}_h| = k = 2\pi/\lambda$ in the S wafer of the LLL interferometer. In this case the boundary conditions on the entrance surface $\mathbf{r}_{S1}(z_{S1} = z_1)$ may be written in the form (Authier & Simon, 1968):*

$$E_o^i(\lambda,\mathbf{r}_{S1}) = \frac{a^i(\lambda)\cos\theta}{4\pi z_1}\exp\left[i\,\frac{k\cos^3\theta}{2z_1}(x_{S1}+z_1\tan\theta)^2\right],$$
$$E_h^i(\lambda,\mathbf{r}_{S1}) = 0. \qquad (A.6)$$

On the exit surface of the S wafer, $\mathbf{r}_{S2}$ ($z_{S2} = z_1 + t_S$) amplitudes E_o^i and E_h^i are defined by the influence of the field (*A*.6) and are expressed through equation (*A*.3). Let us consider the spherical approximation condition $z_1 \ll t_S\sin^2 2\theta/2\chi \simeq 10m$ to be fulfilled.† In this case, the integral in (*A*.3) is calculated by the method of a steady-state phase in the vicinity of the point $x' \simeq -z_1\tan\theta$:

$$E_o^i(\lambda,\mathbf{r}_{S2}) = -4a^i(\lambda)\chi P_2 G_o(x_{S2}+z_1\tan\theta,t_S),$$
$$E_h^i(\lambda,\mathbf{r}_{S2}) = 4a^i(\lambda)\chi_h P_2 G_o(x_{S2}+z_1\tan\theta,t_S),$$
$$\text{where } P_2 = (128\pi k z_1\cos\theta)^{-1/2}\exp(i\pi/4). \qquad (A.7)$$

* We neglect the δ-like singularities in functions G_{oo} and G_{hh} (δ is the Dirac function), since they correspond to the kinematic approximation of the diffraction theory and are essential only for the crystal thickness of the order of $l_o/2\sqrt{2\pi} = 1$–10 μm.

* If $\cos\psi \neq 1$ then in equations (*A*.6)–(*A*.19) all the parameters which are measured in the **OZ** direction (such as t_S, t_M, t_A, T, b_1, b_2, z_1 and z_3) should be divided by $\cos\psi$.

† Dynamical diffraction of monochromatic waves by a single crystal in the case of large distances ($\sim t\sin^2 2\theta/2\chi$) between the source and the observation point has been considered theoretically by Afanasjev & Kohn (1977) and experimentally by Aristov, Polovinkina, Shmytko & Shulakov (1978).

Let us assume that the wavefield in the air gaps between the interferometer wafers is also determined by equations (*A*.2) with $\alpha = 0$† and by the influence functions $G_{oo} = \delta(z\tan\theta + x)$, $G_{hh} = \delta(z\tan\theta - x)$, $G_{ho} = G_{oh} = 0$. Thus, after passing the air gap b_1 the waves E_o^i and E_h^i reach mirror $M(z_{M1} = z_1 + t_S + b_1)$ with the displacements $-b_1\tan\theta$ and $b_1\tan\theta$ respectively (Indenbom, Slobodetsky & Truni, 1974):

$$E_o^i(\lambda,\mathbf{r}_{M1}) = -4a^i(\lambda)\chi P_2 G_o(x_{M1} + z_1\tan\theta + b_1\tan\theta, t_S),$$
$$E_h^i(\lambda,\mathbf{r}_{M1}) = 4a^i(\lambda)\chi_h P_2 G_o(x_{M1} + z_1\tan\theta - b_1\tan\theta, t_S). \quad (A.8)$$

If we assume that wafers S and M are not shifted relative to each other and that their reciprocal lattices coincide, then the amplitudes of the fields E_{oh}^i and E_{ho}^i on the exit surface of mirror $M(z_{M2} = z_1 + t_S + b_1 + t_M)$ are determined by equations (*A*.3) and (*A*.8). Convolutions of $G_o * G_o$ in (*A*.3) are calculated by the method of a steady-state phase in the vicinity of points $x' = [x_{M2}t_S - (z_1 \pm b_1)t_M\tan\theta]/(t_S + t_M)$:‡

$$G_o(x_{M2} - x', t_M) * G_0(x' + z_1\tan\theta \pm b_1\tan\theta, t_S) = (\tfrac{1}{2}\chi)\,G_o(x_{M2} + z_1\tan\theta \pm b_1\tan\theta, t_S + t_M). \quad (A.9)$$

Thus

$$E_{oh}^i(\lambda,\mathbf{r}_{M2}) = -2a^i(\lambda)\chi_h P_2 G_o(x_{M2} + z_1\tan\theta + b_1\tan\theta, t_S + t_M),$$
$$E_{ho}^i(\lambda,\mathbf{r}_{M2}) = 2a^i(\lambda)\chi P_2 G_o(x_{M2} + z_1\tan\theta - b_1\tan\theta, t_S + t_M). \quad (A.10)$$

On the entrance surface of analyser A $(z_{A1} = z_1 + t_S + b_1 + t_M + b_2)$:

$$E_{oh}^i(\lambda,\mathbf{r}_{A1}) = -2a^i(\lambda)\chi_h P_2 G_o(x_{A1} + z_1\tan\theta - \Delta b\tan\theta, t_S + t_M),$$
$$E_{ho}^i(\lambda,\mathbf{r}_{A1}) = 2a^i(\lambda)\chi P_2 G_o(x_{A1} + z_1\tan\theta + \Delta b\tan\theta, t_S + t_M), \quad (A.11)$$

where $\Delta b = b_2 - b_1$ is the value of the interferometer defocusing.

Suppose values χ_h and $\mathbf{h}$ in wafer A $(\chi_{hA}, \mathbf{h}_A)$ differ from the same parameters in the first two wafers. In this case convolutions of $G * G_o$ are also calculated by the steady-state phase method in the vicinity of the points: $x' = [x_{A2}(t_S + t_M) - (z_1 \mp \Delta b)t_A\tan\theta + (\alpha^j/2\chi)(t_S + t_M)t_A\tan\theta]/T$. Finally, for E_{ohh}^i and E_{hoh}^i on the exit surface of the interferometer $(z_{A2} = z_1 + z_L)$ we may write:

$$E_{ohh}^i(\lambda,\mathbf{r}_{A2}) = a^i(\lambda)\chi_h P_2 G_o(x_{A2} + z_1\tan\theta - \Delta b\tan\theta, T)\exp(i\varphi^{\mathrm{I}}),$$
$$E_{hoh}^i(\lambda,\mathbf{r}_{A2}) = a^i(\lambda)\chi_{hA} P_2 G_o(x_{A2} + z_1\tan\theta + \Delta b\tan\theta, T)\exp(i\varphi^{\mathrm{II}}), \quad (A.12)$$

where

$$\varphi^j = -\alpha^j(kt_A/4T\cos\theta)[x_{A2}\cot\theta + z_1 \mp \Delta b + T - (\alpha^j/4\chi)(t_S + t_M)]. \quad (A.13)$$

Here j = I, II; at j = I the upper sign (minus) is taken, at j = II the lower sign (plus) is taken; α^j is the angular parameter α for the first and second fields (E_{ohh}^i and E_{hoh}^i):

$$\alpha^{\mathrm{I}} = 2(\mathbf{k}_o\Delta\mathbf{h})/k_o^2, \quad \alpha^{\mathrm{II}} = 2(\mathbf{k}_h\Delta\mathbf{h})/k_o^2, \quad (A.14)$$

where $\Delta\mathbf{h} = \mathbf{h}_A - \mathbf{h}$.

Waves E_{ohh}^i and E_{hoh}^i interfere on the exit surface of the interferometer, so that the density of the intensity for the ith act of radiation is determined by the expression:

$$\frac{c}{8\pi}|E_{ohh}^i + E_{hoh}^i|^2 = |a^i(\lambda)|^2|E_h^{\mathrm{I}} + E_h^{\mathrm{II}}|^2. \quad (A.15)$$

Here $E_h^{\mathrm{I}} = E_{ohh}^i/a^i(\lambda)$ and $E_h^{\mathrm{II}} = E_{hoh}^i/a^i(\lambda)$ are defined by diffraction in the interferometer and are independent of the radiation act number. On averaging the intensity determined by this expression over all radiation acts for a long period of time, we get:

$$\frac{c}{8\pi}\left\langle \sum_i |E_{ohh}^i + E_{hoh}^i|^2 \right\rangle = \frac{c}{8\pi}\sigma(\lambda)|E_h^{\mathrm{I}} + E_h^{\mathrm{II}}|^2. \quad (A.16)$$

Here angle brackets denote averaging over time, and $\sigma(\lambda) = \langle\sum_i|a^i(\lambda)|^2\rangle$ is the spectral density of the source radiation, the amplitude and phase relations of the interfering waves E_h^{I} and E_h^{II} being determined by the expressions [see equations (*A*.15), (*A*.12), (*A*.7) and (*A*.5)]:

$$|E_h^{\mathrm{I(II)}}(\lambda,\mathbf{r}_{A2})|^2 = |\chi_h|^2|P_1|^2|P_2|^2 \times \exp[-(x_q \mp \Delta b\tan\theta)/\Delta_o^2], \quad (A.17)^*$$

$$\arg\left\{\frac{E_h^{\mathrm{I}}}{E_h^{\mathrm{II}}}\right\} = \arg\left\{\frac{\chi_h}{\chi_{hA}}\right\} + \arg\left\{\frac{G_o(x_q - \Delta b\tan\theta, T)}{G_o(x_q + \Delta b\tan\theta, T)}\right\} + (\varphi^{\mathrm{I}} - \varphi^{\mathrm{II}}), \quad (A.18)$$

† Such a condition allows us not to write the boundary conditions on the surfaces of the interferometer wafers.

‡ The applicability of the steady-state-phase method in the Borrmann approximation follows from the fact that far from the absorption edges $|\chi'| \gg |\chi''|$ and the phase rapidly oscillates inside the region with dimensions of the order of $2\Delta_o$.

* In deriving formula (*A*.17) we neglected divergence of the diffracted rays in the **OY** direction. If this is taken into consideration, the intensities of fields $|E_h^{\mathrm{I(II)}}|^2$ decrease by the coefficient $z_1/(z_1 + z_L)$.

where x_q is determined from equation (6) at $z_3 = -z_1$ and equals $x_{A2} + z_1 \tan\theta$; the value $\Delta_o = \Delta_o(T)$ is determined in equations (A.5) and (9).

In calculating the amplitudes of fields $E_h^{\rm I}$ and $E_h^{\rm II}$ we omitted the time dependence. If the phase difference arises when a phase object is put into the path of one of the beams, then fields $E_h^{\rm I}$ and $E_h^{\rm II}$ reach the point $\mathbf{r}_{A2}$ at different moments of time τ and $\Delta\tau$. In this case an additional phase difference $\Phi(\Delta\tau) = \omega\Delta\tau$ appears. Let us express ω through x_q, then:

$$\Phi(\Delta\tau) = \bar{\omega}\Delta\tau(1 + x_q \cos^3\theta/z_3 \sin\theta), \quad (A.19)$$

where $\bar{\omega}$ is the mean value of the cyclic frequency of waves reaching the observation point within the variation range $|x_q| \lesssim \Delta_o$.

References

AFANASJEV, A. M. & KOHN, V. G. (1977). *Fiz. Tverd. Tela (Leningrad)*, **19**, 1775–1783.

ARISTOV, V. V. (1978). *Proceedings of the Ninth All-Union Holography School*, pp. 299–312. Leningrad: Institute of Nuclear Physics.

ARISTOV, V. V., POLOVINKINA, V. I., SHMYTKO, I. M. & SHULAKOV, E. V. (1978). *Pis'ma Zh. Eksp. Teor. Fiz.* **28**, 6–9.

ARISTOV, V. V., SHMYTKO, I. M. & SHULAKOV, E. V. (1977*a*). *Acta Cryst.* A**33**, 418–423.

ARISTOV, V. V., SHMYTKO, I. M. & SHULAKOV, E. V. (1977*b*). *Acta Cryst. A***33**, 412–418.

ARISTOV, V. V. & SHULAKOV, E. V. (1975). *J. Appl. Cryst.* **8**, 445–451.

AUTHIER, A. & SIMON, D. (1968). *Acta Cryst. A***24**, 517–526.

BONSE, U. & HART, M. (1965). *Appl. Phys. Lett.* **6**, 155–156; *Z. Phys.* **188**, 154–164.

BONSE, U. & TE-KAAT (1971). *Z. Phys.* **243**, 14–45.

BORN, M. & WOLF, E. (1964). *Principles of Optics*. New York: Pergamon Press.

DWIGHT, H. B. (1961). *Tables of Integrals and Other Mathematical Data*. New York: Macmillan.

GEVERS, R. (1962). *Philos. Mag.* **7**, 1681–1720.

INDENBOM, V. L. & CHUKHOVSKY, F. N. (1972). *Usp. Fiz. Nauk*, **107**, 229–265.

INDENBOM, V. L., SLOBODETSKY, I. SH. & TRUNI, K. G. (1974). *Zh. Eksp. Teor. Fiz.* **66**, 1110–1120.

HART, M. (1968). *Br. J. Appl. Phys.* **1**, 1405–1408.

PINSKER, Z. G. (1974). *Dynamic Scattering of X-rays in Ideal Crystals* (in Russian). Moscow: Nauka.

SHULAKOV, E. V. & ARISTOV, V. V. (1978). *Proceedings of the All-Union Conference on X-ray Multiwave Scattering*, pp. 129–137. Univ. of Erevan.

SLOBODETSKY, I. SH., CHUKHOVSKY, F. N. & INDENBOM, V. L. (1968). *Pis'ma Zh. Eksp. Teor. Fiz.* **8**, 90–94.

TAKAGI, S. (1962). *Acta Cryst.* **15**, 1311–1312.

Acta Cryst. (1979). A**35**, 213–220

Derivation of Three-Phase Invariants from the Patterson Function

BY G. ALLEGRA

Istituto di Chimica, Piazza Leonardo da Vinci 32, *Politecnico*, 20133 *Milano, Italy*

(*Received* 1 *March* 1978; *accepted* 22 *August* 1978)

Abstract

The idea of Anzenhofer & Hoppe [*Phys. Verh.* (1962), **13**, 119] that all the Fourier coefficients of the function $\rho(\mathbf{r}).\rho(\mathbf{r} + \mathbf{u})$ are zero if the Patterson function is zero at vector point $\mathbf{u}$ is first developed; it is shown that the three-phase cosine and sine invariants may be derived jointly by solving two sets of linear equations. A least-squares method exploiting the entire Patterson function is then presented; this may allow the three-phase cosine and sine invariants to be determined and/or refined. As expected, the low-valued Patterson regions contribute most to the least-squares procedure.

0567-7394/79/010213-08$01.00

Introduction

Anzenhofer & Hoppe (1962) first pointed out that, if the Patterson function $P(\mathbf{u})$ of any structure is zero at some vector point $\mathbf{u}$, exact equations among structure factors may be derived. In fact, the shift-product function $\rho(\mathbf{r}).\rho(\mathbf{r} + \mathbf{u})$ must be zero for any $\mathbf{r}$; consequently, all its Fourier components must vanish, thus producing a set of linear equations among products of structure factor pairs (Anzenhofer & Hoppe, 1962; Hoppe, 1962, 1963). More recently, Dideberg (1977) also discussed applications of the same idea. It is interesting to recall that Main & Woolfson (1962, 1963)